J. Fluid Mech. (1996), *vol.* 322, *pp.* 329–353
Copyright © 1996 Cambridge University Press

Interaction of single travelling bubbles with the boundary layer and attached cavitation

By CHIH-YANG LI AND STEVEN L. CECCIO

Mechanical Engineering and Applied Mechanics, University of Michigan, Ann Arbor, MI 48109, USA

(Received 31 July 1995 and in revised form 16 April 1996)

Individual travelling cavitation bubbles were examined as they interacted with the flow over a two-dimensional hydrofoil. Each bubble was produced from a single nucleus created upstream of the hydrofoil, and the flow near the hydrofoil was visualized using particle imaging velocimetry (PIV). Travelling bubbles were observed to generate a local region of turbulence as they passed close to an unstable laminar boundary layer. By producing a locally turbulent region, the bubbles could temporarily sweep away a portion of attached cavitation at the foil midchord. Also, the bubbles were observed to strongly interact with a turbulent boundary layer, producing local regions of patch cavitation.

1. Introduction

In this study we examine physical processes through which nuclei and the viscous flow can influence the inception and form of travelling bubble and sheet cavitation. Much of the research into the fundamental mechanisms of cavitation has been motivated by the existence of cavitation scale effects. The inception conditions, appearance, and acoustic emission of cavitation can differ widely between a model and a larger, but geometrically similar, prototype. Viscous or Reynolds number scale effects were explored by Arakeri & Acosta (1973), Arakeri (1975), Huang & Peterson (1976), van der Meulen (1980), and Franc & Michel (1985 & 1988). These studies focused primarily on attached cavitation inception and its relationship with boundary layer separation. Viscous scaling effects associated with bubble cavitation were examined by Kuhn de Chizelle, Ceccio & Brennen (1995).

The inception of cavitation can be significantly influenced by the 'quality' of the liquid in the cavitating flow. By this, researchers usually mean the degree to which the liquid can sustain tension before cavitating. Liquid quality is strongly dependent upon both its free and dissolved gas content. The influence of nuclei population on the inception of bubble cavitation is well understood and has been examined by Ceccio & Brennen (1991), Meyer, Billet & Holl (1992), and Liu & Brennen (1994). Recent experimental studies of hydrodynamic bubble cavitation include van der Meulen & Renesse (1989), Ceccio & Brennen (1991), and Kuhn de Chizelle *et al.* (1995), and a review, including theoretical treatments, is provided by Brennen (1995). The influence of nuclei on attached cavitation has been examined by Franc & Michel (1985 & 1988), and Briançon-Marjollet, Franc & Michel (1990) observed how varying nuclei content influenced the inception of sheet cavitation. A recent review of cavitation inception mechanisms is provided by Rood (1991).

It is not clear that varying nuclei populations will influence sheet cavitation inception. Kuiper (1981) determined that inception on a propeller designed to experience leading-edge sheet cavitation can be delayed only if there are very few free-stream nuclei present. The same propeller geometry was also tested by Gindroz & Billet (1994) who found that inception of leading-edge sheet cavitation was influenced little by variation in the free-stream nuclei content, and Weitendorf & Tanger (1993) found similar results regarding sheet cavitation inception on model propellers. These results can be contrasted with those of Kodoma, Tamiya & Kato (1978) where attached cavitation on an axisymmetric headform was observed to evolve into a bubble cloud as the free-stream nuclei distribution was increased, and similar results can be inferred from the data of Gates *et al.* (1979) for inception on axisymmetric headforms. Briançon-Marjollet *et al.* (1990) reported a mechanism through which nuclei content can influence the formation of attached cavitation: travelling bubbles were observed 'sweeping' away attached cavitation. The authors demonstrated that attached cavitation could be entirely replaced by bubbly cavitation solely through changes in the free-stream nuclei content. Although several mechanisms were suggested, the details of the interaction were unresolved.

Almost the opposite of bubble sweeping was observed during the experiments of Kuhn de Chizelle *et al.* (1995) in which cavitation on axisymmetric headforms of varying sizes was examined. On the small headform, distinct hemispherical bubbles were observed, but as the size of the headform was increased, the occurrence of individual bubbles was reduced. Instead, bubbles were often associated with regions of local attached cavitation which formed upstream of the bubble. Moreover, many bubbles evolved into regions of local patch cavitation, and for the largest headform, only transient patches were commonly observed. For some flow conditions, all of these various types of travelling cavitation appeared simultaneously.

In the present study we examine the underlying physical processes through which transient cavitation events can interact with the viscous flow near the cavitating surface and with attached cavitation. Individual travelling cavitation events were controllably produced, and the resulting flow was examined in detail. We examine the process by which travelling bubbles evolve into local regions of patch cavitation and the process by which travelling bubbles interact with attached cavitation. Lastly, we discuss the mechanisms through which travelling bubbles interact with the boundary layer.

2. Experimental set-up

2.1. *Cavitation tunnel and models*

A detailed description of the cavitation facility and techniques employed in this study is provided in Tassin *et al.* (1995), and only a brief description is presented here. The experiments were conducted in the Blow Down Water Tunnel (BDWT) of the Cavitation and Multiphase Flow Laboratory at the University of Michigan. The BDWT consists of two 1.51 m^3 water tanks joined by an pipe system with a maximum diameter of 20.3 cm. The square test section is 76.2 mm wide and 419 mm high and is located beneath the upper tank. A square contraction nozzle of area ratio 4.4 connects the test section with the upper tank, and the flow enters a diffuser downstream from the test section. Both tanks are connected to pressure and vacuum lines via electrically actuated valves which are used to set the test section velocity and static pressure during operation. To begin a blowdown sequence, a slight pressure

difference is applied to the water tanks to slowly move the water into the upper tank. Next, the water is allowed to settle for at least 10 to 20 minutes to provide time for small gas bubbles to rise to the free surface in the tanks. Flow is initiated in the test section by suddenly applying a pressure difference across the free surfaces in the two tanks. The ultimate test section velocity, U_o , and inlet static pressure, P_o, are adjusted by varying the initial pressure in the tanks and the flow rate through the pressure and vacuum lines. It is possible to maintain a constant flow rate and pressure over a significant period of the blowdown through control of the pressure and vacuum valves. In these experiments, the quasi-steady free-stream velocity ranges between 10 and 15 $\mathrm{m\,s^{-1}}$, and the cavitation number, σ_v, defined as $\sigma_v = 2(P_o - P_v)/\rho U_o^2$, ranges between 0.28 and 1.38, where P_v is the liquid vapour pressure and ρ is the liquid density. After the initiation of a blowdown, the water tunnel test section velocity becomes quasi-steady, and the velocity will decelerate at a rate of approximately 0.1 $\mathrm{m\,s^{-2}}$ during the blowdown. Also, by allowing the water settle before a blowdown, a very low free-stream turbulence level can be achieved.

The two-dimensional hydrofoil used in this study has a NACA 63_1A012 section profile of 82.8 mm chord with a maximum thickness of 12% located at 35% of chord measured from the leading edge. The hydrofoil is mounted on a test section window using a flush-mounted arbor, and the spanwise width of the foil is slightly less than 76.2 mm, the width of the test section. The hydrofoil tip on the unmounted window side is rounded to avoid cavitation from the window wall since such wall-side cavitation would block the profile view of the flow. The hydrofoil is fabricated out of brass and is highly polished, and the surface is coated with black chrome to reduce optical reflectivity.

2.2. *Nuclei control and production*

Control of the ambient nuclei population in the BDWT is necessary to prevent randomly occurring cavitation events from dominating the flow. To remove the naturally occurring nuclei, the water was de-aerated under vacuum for several hours before a series of blowdowns, reducing the oxygen content to approximately 20% saturation at atmosphere pressure. The water was allowed to settle for 10 to 20 minutes before each blowdown so that small gas bubbles could rise to the free surfaces in the water tanks. In this way, it was possible to create flows without any travelling cavitation.

A single nucleus was then produced at a desired location in the flow with a focused pulse of laser light. A frequency-doubled Quantel 581C Nd-YAG laser was used to induce a single nucleus, and the light pulse was focused slightly upstream from the leading edge of the hydrofoil after being relayed through the appropriate optics. By applying approximately 140 mJ/pulse at the focal point, a nucleus is generated through rapid vaporization of water in the small focal region. A microscopic gas bubble resulting from diffusion is then convected over the foil into the low-pressure region, producing a macroscopic cavitation bubble. A schematic diagram of the optical set-up is shown in figure 1(*a*).

2.3. *Flow visualization*

Still images of the cavitating flow were captured using open-shutter flash photography, and video images were acquired with a Kodak Ektapro 1000 at a maximum rate of 6000 frames per second. Although the video framing rate was too slow to capture distinct images of the travelling cavitation, it was sufficiently fast to examine some motion of the sheet cavitation.

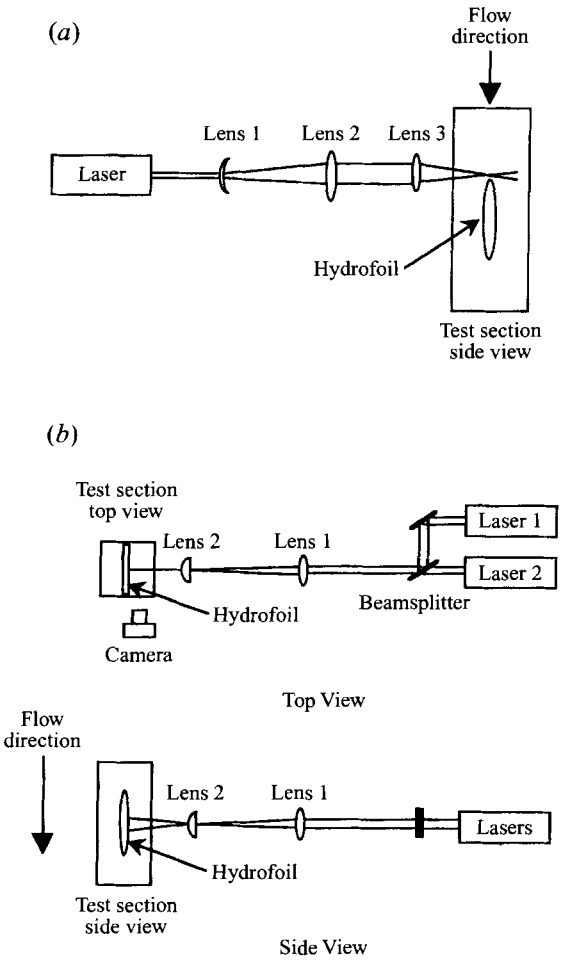

FIGURE 1. A schematic diagram of the optical set-up used (*a*) to produce a single nucleus and (*b*) to acquire images for the particle imaging velocimetry.

The flow near the hydrofoil and associated with the travelling cavitation was examined using particle imaging velocimetry (PIV) (Adrian 1991), and details of the optical set-up are provided in Tassin *et al.* (1995). The flow is first seeded with small particles of titanium dioxide which have a mean diameter of 3 μm, and after the particles were submerged in the de-aerated water for a day or two, any free gas on their surface was dissolved away thus preventing the particles from acting as cavitation nuclei. These particles may be considered Lagrangian flow tracers, and multiple time-delayed images of individual particles were used to determine local velocities in the flow. Doubly exposed images of the particles in a plane of the flow are created by generating a pulsed light sheet with two frequency-doubled Quanta Ray GCR 130 Nd-YAG lasers, and the image created by the light sheet is captured on film. A schematic diagram of the PIV optical set-up is shown in figure 1(*b*). Appropriate delay between the nuclei-producing laser and the PIV system permits the interrogation of the flow around single cavitating bubbles.

The double-pulsed image is captured on film with a magnification factor of 3.44 and is enlarged and printed with a final magnification factor of 43.0. The image is

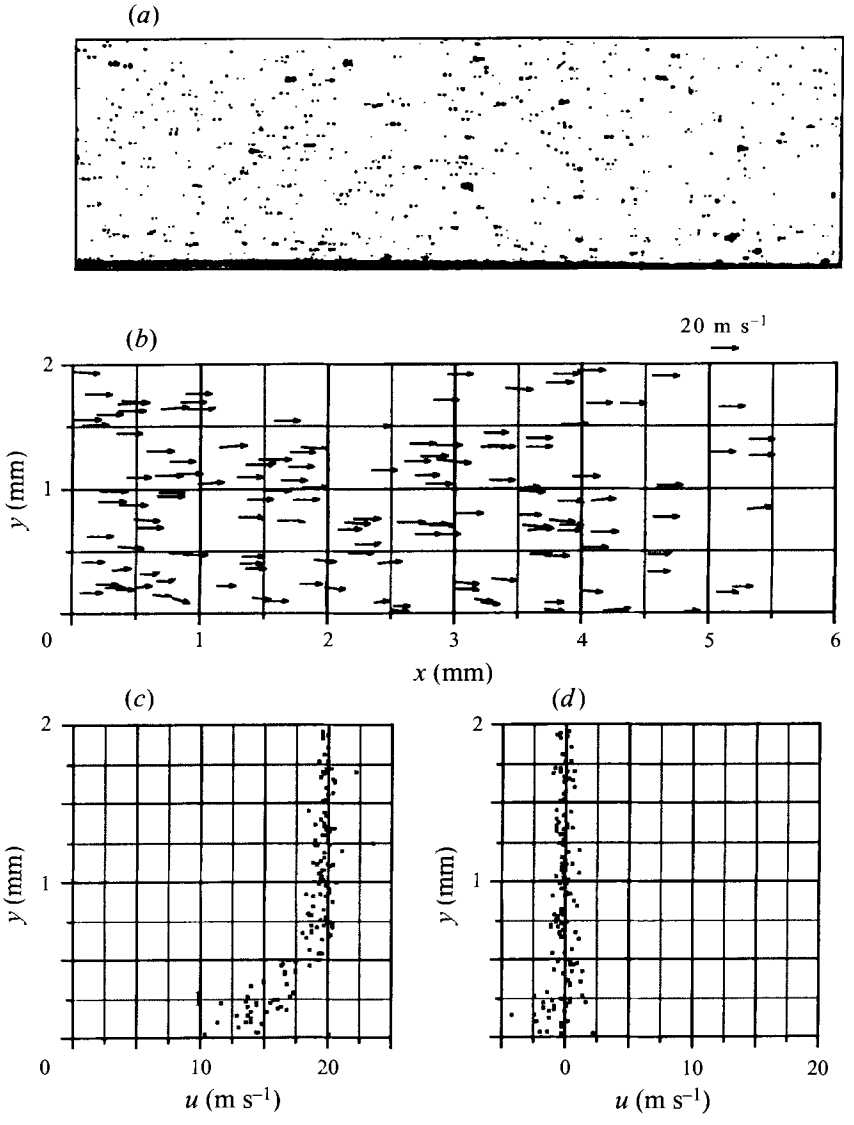

FIGURE 2. The process of data reduction for the PIV images is illustrated. First, an image is acquired of particle trajectories in a plane of the flow parallel to the mean flow direction (*a*). Next, local velocity vectors are derived from the particle trajectories (*b*). Lastly, an assumption is made that the flow is parallel over the interrogation region, and the velocity vectors are then collapsed to produce spatially averaged streamwise velocity (*c*), and transverse velocity (*d*).

then scanned into a digital image file at 600 dpi (optical) and analysed on a Macintosh PowerPC 6100/60 40/250 computer using the program NIH Image 1.57. With this program, the position of each particle is determined by an algorithm which calculates the centre of the best fitting ellipse for each spot. With knowledge of the particle positions and the time delay between exposures, the velocity of the particle is computed. We do not attempt to correct vectors for the possible presence of backward flow (directional discrimination), since backflow is unlikely in the regions of flow under study.

Figure 2 shows different stages of the PIV data acquisition and reconstruction.

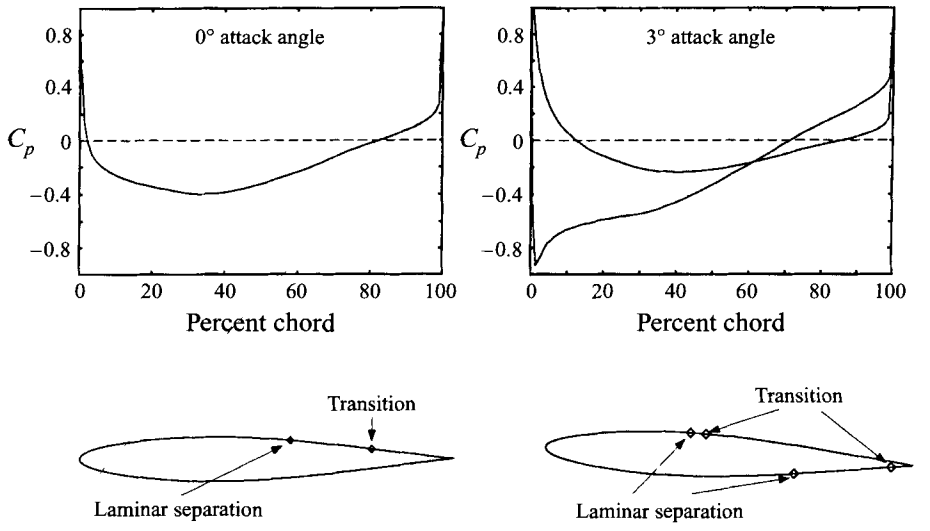

FIGURE 3. The theoretically predicted non-cavitating flow over the NACA 63_1A012 hydrofoil is presented for 0 and 3° attack angles at a Reynolds number of $Re_c = 1.24 \times 10^6$. The two-dimensional potential flow around the hydrofoil within the test section was calculated, and the surface pressure distribution is presented. Next, boundary integral methods were used to calculate the growth of the laminar boundary layer along with the location of laminar separation and boundary layer transition.

Velocity vectors are determined in the analysed flow plane which in the figure measures 6 by 2 mm. To generate a velocity profile near the foil surface, the velocity vectors measured over a small streamwise extent of the flow are collapsed onto a single profile. Thus, we assume that the flow is nearly parallel over the sampled streamwise location, in this case 6 mm. This assumption is justified by noting that the streamwise pressure gradients are changing slowly over the interrogated region.

2.4. *Acoustic measurements*

The acoustic emission of individual travelling cavitation events were detected and recorded. A hydrophone (B & K Type 8103) was mounted inside a window cavity, and an acoustic path was created between the cavitation and the hydrophone through a thin lucite acoustic window. The hydrophone was surrounded with water to complete the acoustic path. No attempt was made to correct for the reverberation of sound within the test section, and the acoustic data are only employed to make a relative comparison between the sound produced by different cavitation events. The signal from the hydrophone was conditioned with a charge amplifier (B & K Type 2635) and then digitized at a sampling rate of 500 kHz. The acoustic emission produced by individual cavitation events was correlated with photographic images taken of the cavitation at its maximum volume.

3. Results: non-cavitating and cavitating flow without travelling bubbles

3.1. *The flow around the non-cavitating hydrofoil*

The non-cavitating flow around the hydrofoil was first examined. Figure 3 shows the surface pressure distribution of the hydrofoil for attack angles 0 and 3° at a free-stream Reynolds number $Re_c = 1.24 \times 10^6$ where Re_c is based on the free-stream velocity

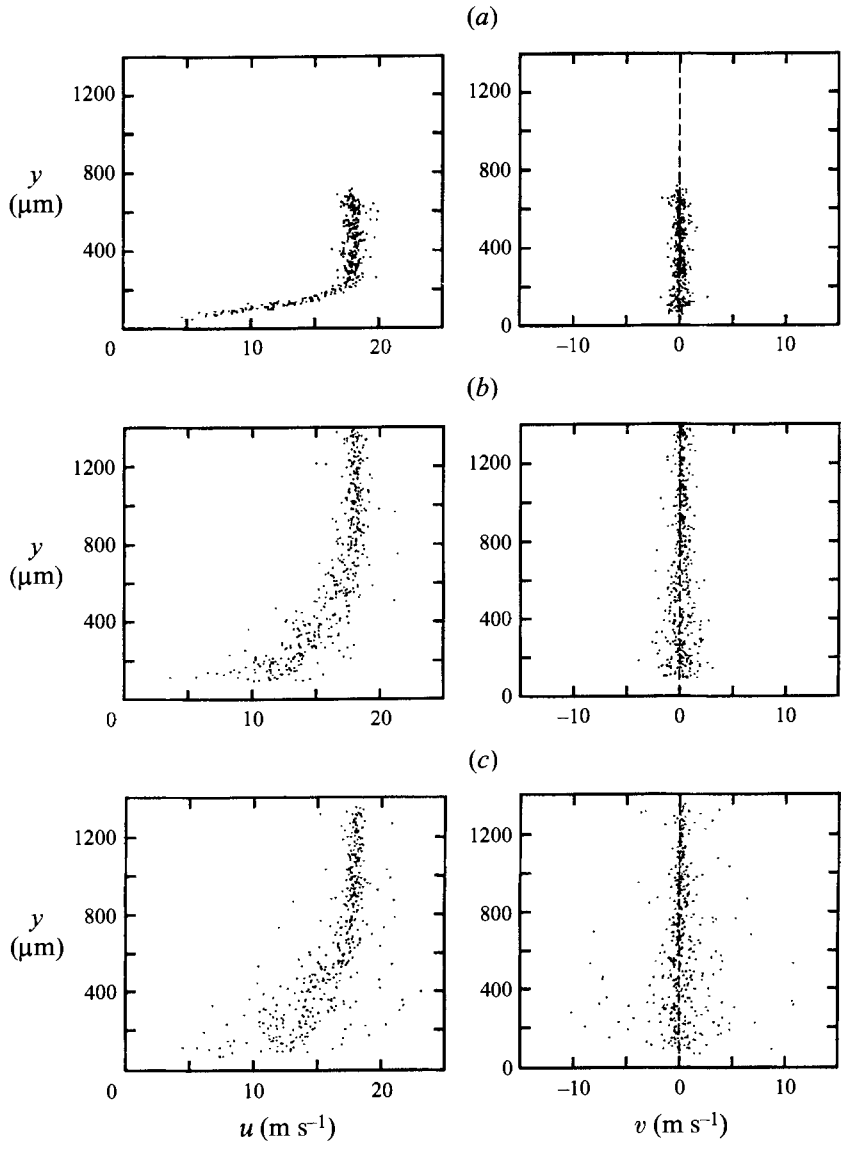

FIGURE 4. The superimposed local velocity measurements taken from several PIV images at the 40% chord location averaged over 3 mm in the mean flow direction. The velocity components parallel to the surface, u, and normal to the surface, v, are shown. The naturally developing boundary layer is shown in (*a*), and two measurements of the stimulated boundary layer are shown in (*b*) and (*c*). In (*b*) the tripping was just sufficient to prevent inception of sheet cavitation, and in (*c*) the maximum tripping was applied.

and the chord length. The two-dimensional potential flow around the hydrofoil was computed including the influence of the test section boundaries, and from this the pressure distribution on the surface of the hydrofoil was determined. The pressure coefficient, C_p, is defined here as $C_p = 2(P_s - P_o)/\rho U_o^2$, where P_s is the pressure on the surface of the hydrofoil. Next, the inviscid velocity distribution on the foil surface was employed in the calculation of the hydrofoil boundary layer thickness using Thwaites method (White 1974). Because the boundary layers are very thin compared with

the distance between the hydrofoil and the wall, the increased blockage due to the hydrofoil boundary layer growth was neglected. Laminar separation was predicted using the Stratford equation, and the region of turbulent transition was estimated using the Granville criterion (White 1974).

For small attack angles, laminar separation is predicted to occur before turbulent transition on the suction side of the hydrofoil, and transition to turbulence is not expected to occur until after the point of maximum thickness. These predictions are consistent with those of Franc & Michel (1985) who examined a two-dimensional hydrofoil with a NACA 16012 section. Both this and the present study have the same maximum thickness (12%) and are symmetric. While the foil section used in this study has maximum thickness at 35% chord, and the 16012 has maximum thickness at 50% chord, the two sections are similar enough for qualitative comparison. In the present experiment, little difference was seen between the 0° and 3° attack angle cases, and results will be presented for the 0° attack angle case.

PIV was used to examine the boundary layer on the suction side of the hydrofoil. Figure 4 presents the velocity vectors near the surface of the hydrofoil at the 40% chord location. The measurements are collected over a distance of 3 mm in the mean flow direction, and the streamwise velocity components, u, and the flow component perpendicular to the foil surface, v, are shown. Three flow conditions are represented: the naturally developing boundary layer (*a*), the stimulated boundary layer with a roughness level which was just sufficient to prevent attached cavitation at the lower cavitation number (*b*), and the stimulated boundary layer with maximum roughness (*c*). As predicted, the unstimulated boundary layer (*a*) has not yet undergone transition. To stimulate the boundary layer, a uniform strip of paint was applied at a location 3.5% of the chord from the leading edge, and the maximum thickness of the strip was 50 μm. The flow resulting from this level of tripping is shown in (*c*). Next, the thickness of the paint layer was reduced to 20 μm which was the minimum thickness necessary for the prevention of attached cavitation, and flow at this level of thickness is shown in (*b*). As can be seen, the turbulent boundary layers are thicker and the profile is changed. A comparison of the naturally developing laminar boundary layer and artificially tripped turbulent boundary layers derived from averaging many data sets is shown in figure 5 using non-dimensional coordinates. The velocities are normalized with the velocity at the edge of the boundary layer, U_e, and the distance above the surface is normalized with the boundary layer thickness, δ. The boundary layer profiles are presented along with the RMS value of the velocity fluctuations in the streamwise and normal directions. As expected, the shapes of the laminar and turbulent boundary layers are consistent with the classically expected profiles with a much higher velocity gradient near the wall for the turbulent flows, and the turbulent boundary layers have much larger velocity fluctuations. Moreover, the two stimulated boundary layer profiles are similar, but the intensities of the turbulent fluctuations differ. The laminar boundary layer data have been fitted with the Pohlhausen polynomial with computed shape factor $H = 2.64$ at the 40% chord and the fully turbulent boundary layer data have been fitted with a logarithmic profile.

3.2. *The flow around the hydrofoil with attached cavitation*

Next, the free-stream cavitation number was reduced to $\sigma_v = 0.4$ and an attached cavity developed. The leading edge of the cavity was located at a position 46.5% chord from the leading edge of the hydrofoil, and the location of inception and the inception cavitation number did not vary with changes in dissolved air content. Figures 6(*a*) and 6(*b*) shows plan and side views of the cavity detachment region.

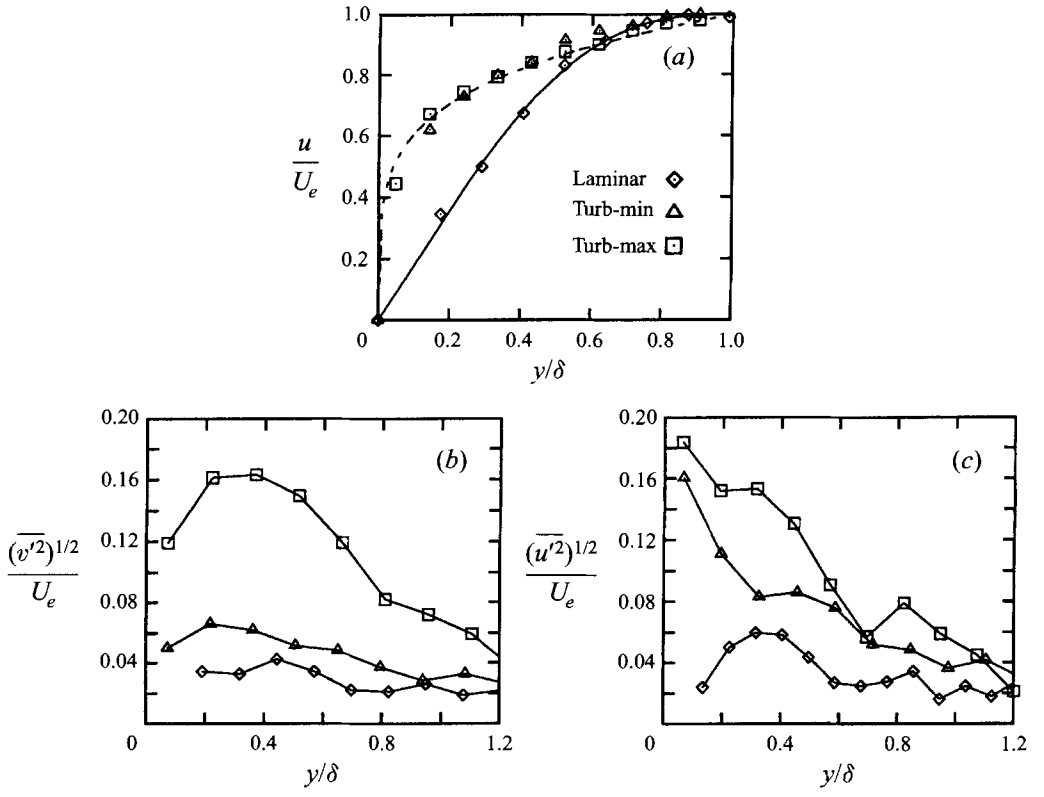

FIGURE 5. The velocity measurements shown in figure 4 are averaged and replotted in non-dimensional coordinates. The boundary layer profiles are shown in (*a*), and the RMS velocity fluctuations in the streamwise direction, u', and in the direction normal to the surface, v', are shown in (*b*) and (*c*). The naturally developing boundary layer is shown along with two stimulated boundary layers representing the case of maximum tripping and tripping just sufficient to prevent the formation of attached cavitation. Also plotted are the fitted velocity profiles for the laminar and fully turbulent boundary layers.

The cavity detaches along a spanwise line, and begins as a series of clear vapour 'fingers' that appear to be separated by thin streamwise regions of liquid. These structures are reminiscent of those observed by Savage (1977*a*, *b*) for cavitation in the gaps of bearings. Shortly after the point of inception, streamwise waves develop on the interface of the finger cavities and the interface ultimately becomes turbulent in a process described by Brennen (1970). A high-speed video shows that the cavity fingers slowly merge and separate, although some remain stable for relatively long time periods. The spanwise speed of the finger motions ranges from 5 to 10% of the free-stream velocity. Observations of the cavity from the side indicate that the finger cavities are approximately 250 μm thick, which is on the order of the boundary layer thickness upstream of the cavity. As shown in figure 6(*c*), the cavity surface near the detachment point is neither tangent nor normal to the surface. Instead, the interface of the finger cavity is approximately parallel to the solid surface and sharply curves toward the surface at the point of cavity detachment.

The location of cavity separation is upstream of any predicted boundary layer separation of the fully wetted flow. The interface of the finger cavities is initially smooth which suggests that the boundary layer immediately upstream of the cavity

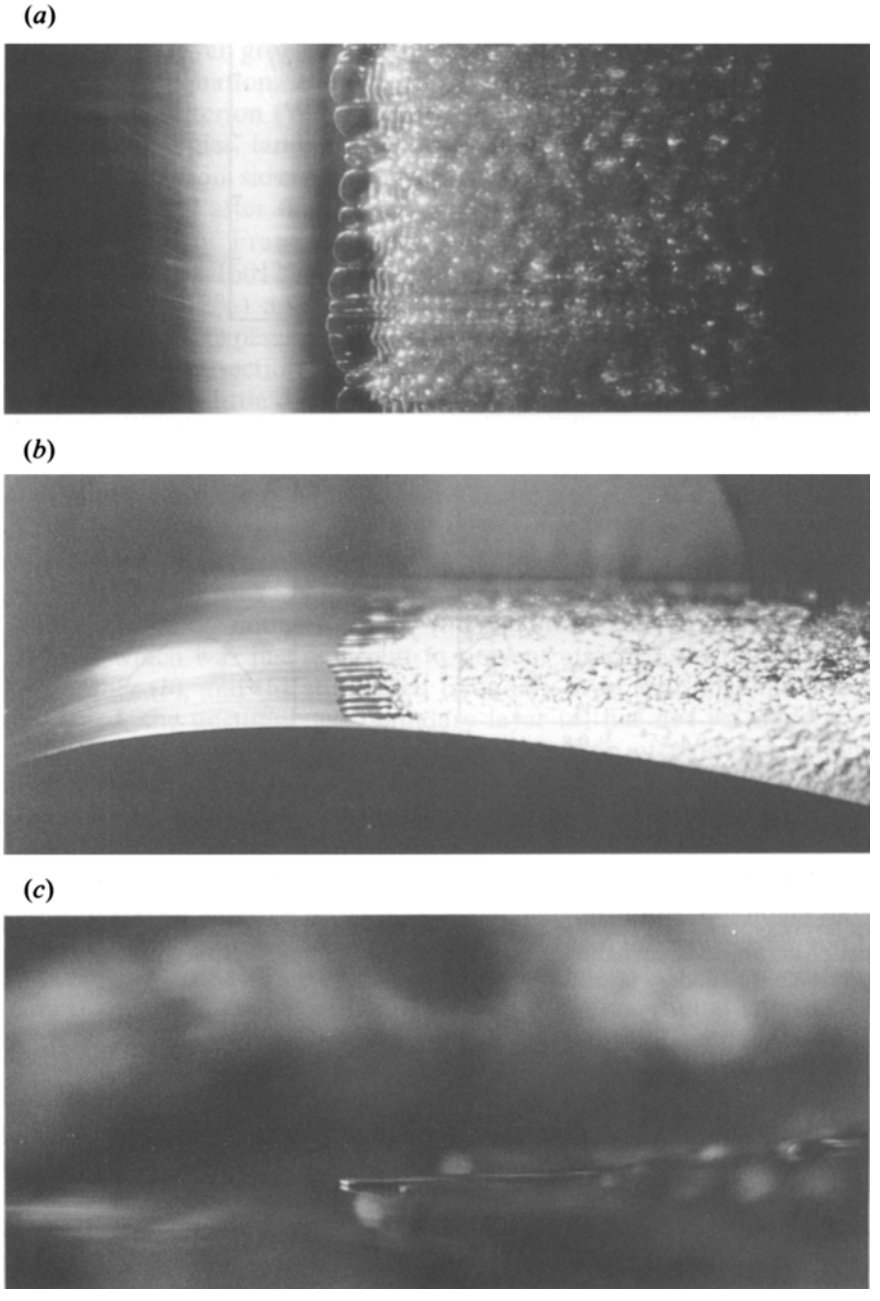

FIGURE 6. Three views of the inception region of the stable attached cavity which occurred near the midchord of the hydrofoil. The plan and side views reveals the 'fingers' which make up the leading edge of the cavity (*a*) and (*b*). A close-up side view of the cavity fingers shows the sharp radius the cavity interface makes with the solid surface (*c*).

has not undergone a transition to turbulence. These results can be compared to those of Franc & Michel (1985) where for small attack angles the position of cavity detachment was close to the predicted region of laminar separation. It is expected that the boundary layer undergoes laminar separation upstream of the cavity separation (Brennen 1969; Arakeri 1975; Franc & Michel 1985), and the geometry of the attached cavity leading edge shown in figure 6(*b*) suggests that there may be a region of separated flow very close to the point where the liquid–vapour interface of the attached cavity leaves the solid surface.

Cavity inception was suppressed after roughness was applied to the hydrofoil leading edge. Transition to turbulence is induced in the boundary layer near the foil, and laminar separation is inhibited. Without the laminar separation, the cavity is prevented from forming. The boundary layer was tripped by applying a thin line of paint to the leading 3.5% of the chord. Strips of varying thickness were employed with the thickest being 50 μm, and care was taken that the strips themselves did not produce local roughness-induced cavitation. Application of the thickest strip stimulated transition to turbulence on the boundary layer, and the attached cavity did not form. Next, the thickness of the strip was slowly reduced until the cavity reappeared. After the interactions between the attached cavities and turbulent boundary layers were observed, PIV images were taken at a slightly higher cavitation number to avoid the formation of small bubbles in the turbulent eddies of the boundary layer.

4. Results: interaction of travelling cavitation with the non-cavitating flow

4.1. *Growth of bubbles travelling over an untripped boundary layer*

A small bubble was generated slightly upstream of the hydrofoil leading edge, and the location of the generated nucleus was varied such that the nucleus would travel near the foil surface on different streamlines. The nucleus was convected into the tension region on the suction side of the hydrofoil and would then cavitate, producing a visible cavitation bubble. The bubbles were hemispherical 'caps', which are commonly observed (see, for example, Ellis 1952, and more recently Briançon-Marjollet *et al.* 1990, and Ceccio & Brennen 1991). The process by which nuclei grow into travelling bubbles is well understood and will not be reviewed here (for a summary, see Brennen 1995).

Figure 7(*a*) shows a series of photographs representing bubbles at various stages of their growth over the hydrofoil and figure 7(*b*) shows a schematic diagram of the growth process. The pattern of bubble growth is similar to that observed by Ceccio & Brennen (1991) for bubble cavitation on axisymmetric bodies. PIV images indicate that the bubbles are travelling at nearly the same speed as the inviscid outer flow, and the volume of the bubbles grows slowly as it moves toward the midchord of the foil. The interface of the cap-shaped bubbles remains clear until the bubbles pass over the midchord region, where the surface of the bubble closest to the foil boundary becomes roughened as it interacts with the turbulent flow of the boundary layer.

Figure 8 presents close-up side images of typical travelling bubbles. When the nuclei are convected on streamlines close to the hydrofoil, the resulting cavitation bubbles are separated from the surface of the hydrofoil by a wedge of liquid, and at its thickest the wedge is on the order of the boundary layer thickness (figure 8(*a*)). Nuclei produced on streamlines moving farther away from the hydrofoil surface produce bubbles which are completely separated from the surface by a relatively

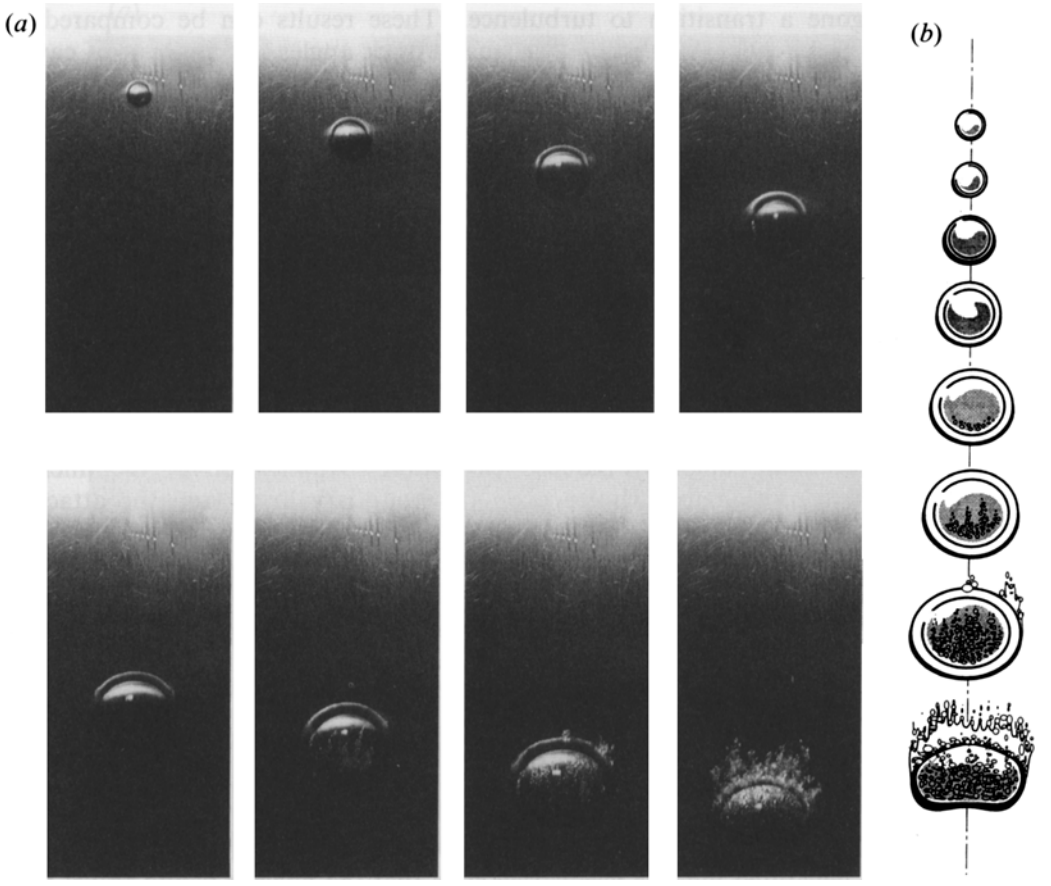

FIGURE 7. (*a*) Plan view of several bubbles as they pass over the naturally occurring boundary layer on the hydrofoil. The bottom surface of the bubbles remains undisturbed until the bubbles pass over the region where the boundary layer is expected to have undergone turbulent transition. (*b*) A schematic diagram of the growth process in (*a*).

thick region of liquid, and the bottom surfaces of the bubbles are nearly parallel to the solid body (Figure 8b). Because small nuclei require a significant tension before cavitating, they will usually grow very close to the foil surface where the tension is greatest, and the resulting macroscopic bubble will impinge on the solid boundary. Conversely, large nuclei can cavitate after passing through regions of lower liquid tension located farther from the foil surface, and the resulting bubble is often wholly separated from the solid boundary.

4.2. *Interaction of travelling bubbles with the naturally occurring boundary layer*

As the travelling bubbles move over the hydrofoil surface, turbulent transition is locally stimulated in the boundary layer. This is evident from the dye visualization of Briançon-Marjollet *et al.* (1990), and this phenomenon was also observed in this study using PIV. From these data, figure 9 was developed which suggests how the region of turbulence grows behind the bubble. The turbulent region begins to grow at the lateral sides of the bubble, and as they grow spatially and in intensity, the two regions merge upstream of the bubble. The point at which the regions merge is approximately one to two bubble base diameters upstream. Figure 9 also shows

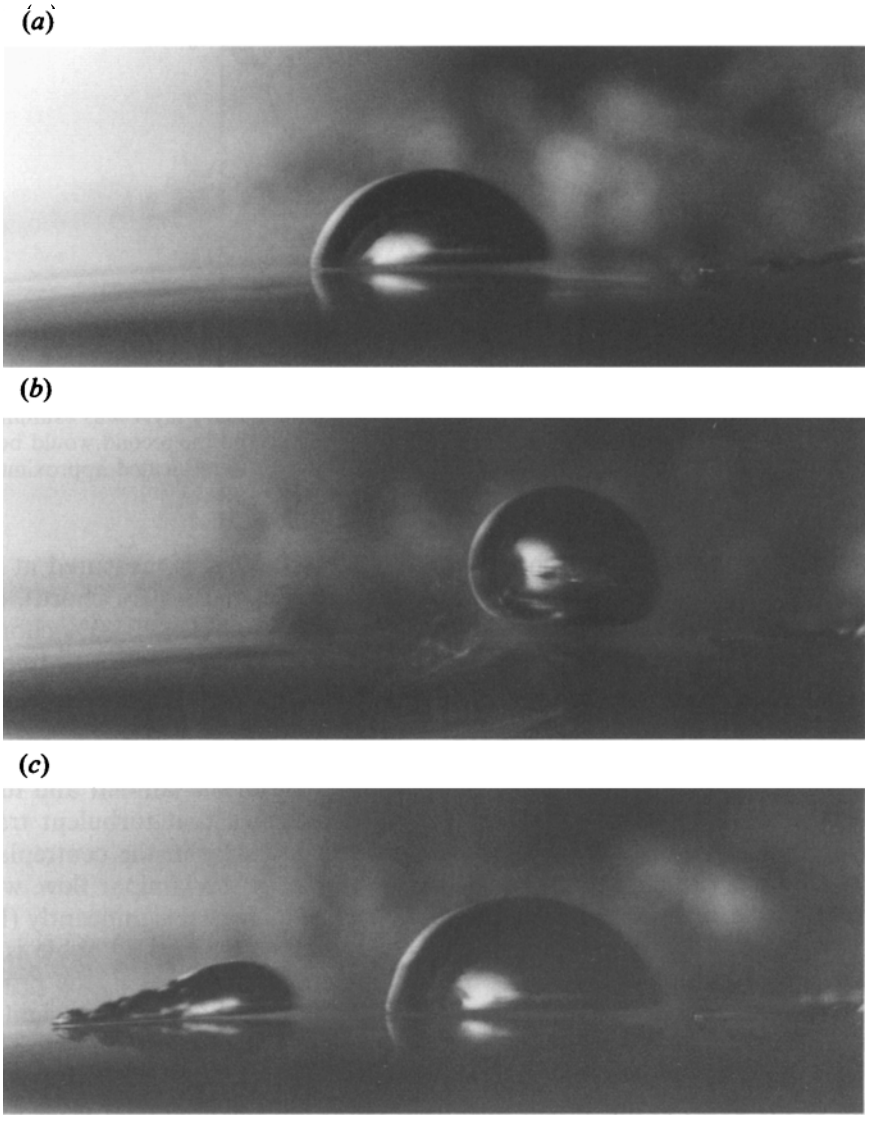

FIGURE 8. Three close-up profile images of travelling bubbles as they pass over the naturally occurring boundary layer on the hydrofoil. The first image shows a bubble travelling close to the solid surface (*a*). The bubble is separated by a 'wedge' of liquid with a maximum thickness on the order of the boundary layer thickness, and the trailing edge of the bubble nearly touches the surface. The second bubble (*b*) is wholly above the solid surface and is separated by a liquid layer with thickness two to three times the boundary layer thickness, and the bottom surface of the bubble is parallel to the foil surface. The last image (*c*) shows a bubble which has formed from a surface nucleus which has been induced on the surface of the hydrofoil leaving a local region of transient partial cavitation.

two streamwise planes upstream of the bubble where PIV images were taken of the boundary layer.

Figure 10 shows the averaged velocity profiles (*a*) and RMS velocity fluctuations in the streamwise direction (*b*) from several PIV images taken upstream of the travelling bubbles. Three conditions are shown. The first two are measured when the bubble

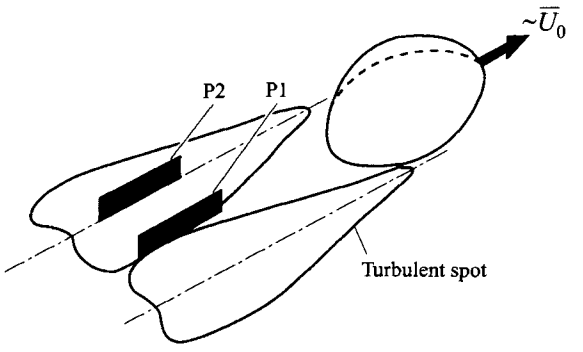

FIGURE 9. Schematic diagram illustrating how two turbulent regions may grow from the spanwise edges of the bubble. Also shown are two planes in which the boundary layer was examined using PIV. The first plane would intersect the centre of the bubble (P1), and the second would be tangent to the spanwise side of the bubble (P2). The centres of the planes were located approximately one bubble base diameter upstream of the bubble trailing edge.

trailing edge is located at 40% chord and, of these, the first is measured at a plane upstream of the bubble which would intersect the bubble (P1-40% chord), and the second is measured at a plane tangent to the side of the bubble (P2-40% chord). The third measurement was taken at the centre plane (P1-45% chord) when the bubble was farther downstream at the 45% chord location. Also plotted are the fitted curves for the laminar and turbulent velocity profiles for the flow without travelling bubbles. The averaged velocity profiles upstream of the bubbles are similar for the three locations upstream of the bubble, and the profile shape lies between the laminar and turbulent profile. Examination of the velocity fluctuations indicates that turbulent transition has been stimulated by the bubbles. The turbulent intensity in the centreplane just behind the bubble (P1-40% chord) is higher than that of the laminar flow, while the fluctuations at the spanwise extent of the bubble have increased significantly (P2-40% chord). The largest fluctuations occur in the centreplane when the bubble is farther downstream (P1-45% chord). These observations are consistent with the production of two turbulent regions suggested in figure 9. Next, we discuss the origin of this turbulent region.

The boundary layer on the suction side of the foil is expected to remain laminar upstream of the point of maximum thickness. However, the boundary layer upstream of the laminar separation can be considered susceptible to disturbances in the flow. The naturally occurring boundary layer at 40% chord as shown in figure 4(*a*) has a measured value of displacement thickness $\delta^* = 80$ μm, and the outer velocity, U_e, is approximately 18 m s^{-1} giving $Re_{\delta^*} = 1440$. The boundary layer profile occurring at this point has a computed shape factor $H = 2.64$ using momentum integral methods. Examination of the neutral stability curve for this boundary layer reveals that the spatial amplification rate of streamwise disturbances is non-zero, indicating that disturbances to the boundary layer will grow (Jaffe *et al.* 1970). Thus, the boundary layer upstream of the maximum chord thickness is unstable to external disturbance even though transition is not yet evident.

We propose the following hypothesis for interaction of a bubble with the boundary layer. The travelling bubble is convected by the potential outer flow and is dragged over the boundary layer. As the bubble travels close to the hydrofoil surface, it squeezes the boundary layer, and mass continuity requires that boundary layer liquid must be expelled from the spanwise sides of the bubble. This flow perturbs the

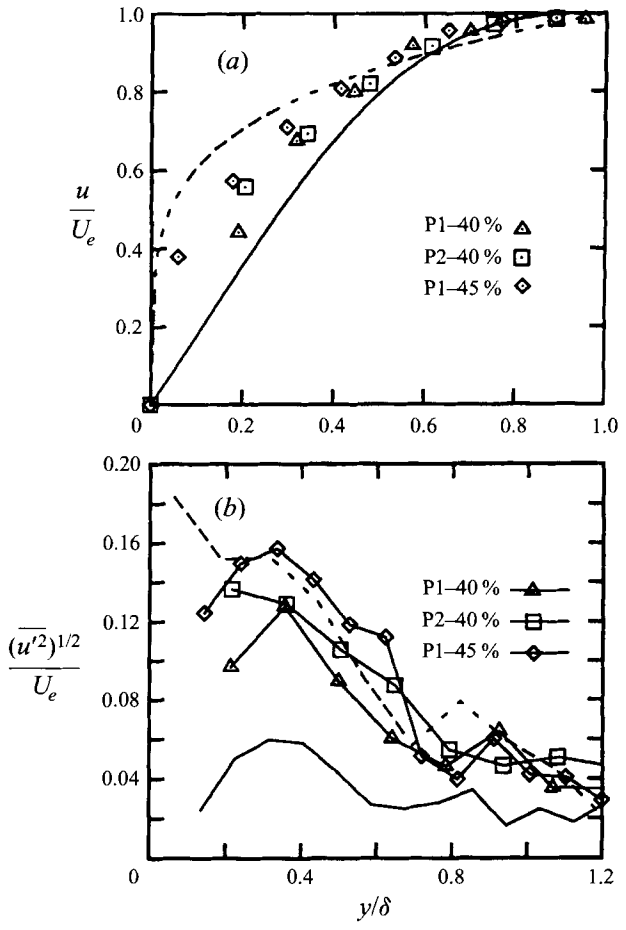

FIGURE 10. The averaged velocity profiles (*a*) and RMS velocity fluctuation in the streamwise velocity component (*b*) are shown for three boundary layers measured upstream of several bubbles, and the location of the planes are shown in figure 9. The first two measurements were taken when the bubble was at 40% chord (P1-40% and P2-40%) and the last when the bubble was at 45% chord (P1-45%). Also plotted is the laminar velocity profile (solid line) and the stimulated turbulent velocity profile (dashed line) which exist without the presence of the travelling bubbles.

vorticity distribution in the otherwise laminar, parallel boundary layer which may be visualized as a series of parallel, spanwise vortex lines. As the bubble passes over the boundary layer, the spanwise flow distorts these vortex lines to create streamwise vorticity, and on the spanwise edges of the bubble, quasi-streamwise vortices are stretched and intensified. Ultimately these streamwise vortices induce a local transition to turbulence through the production of two turbulent spots on the spanwise edges of the travelling bubble, as shown schematically in figure 11. The development of the turbulent spots occurs quickly and within a limited space (for a detailed description of the generation turbulent spots see for example Hinze (1975), Wygnanski, Sokolov & Friedman (1976), and Cantwell, Coles & Dimotakis (1978)). These turbulence spots sometimes entrain the edges of the travelling bubble and induce locally three-dimensional detachments, which may fill with vapour, and this phenomena is usually visualized as bubble 'tails'. Large travelling bubbles are often associated with local patch cavitation which first appears as tails at the lateral sides

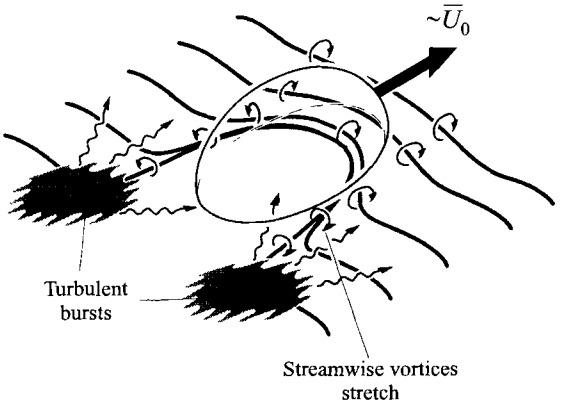

FIGURE 11. A schematic diagram illustrating how the bubble disturbs the boundary layer is shown. Bubbles which travel close to the hydrofoil surface (as shown in figure 8*a*) squeeze boundary layer fluid as they are convected over the boundary layer at nearly the free-stream velocity. This produces spanwise flow in the boundary layer, which is susceptible to disturbances, and results in the local production of a turbulent region.

of the bubble (Ceccio & Brennen 1991). Figure 12 shows a schematic diagram of the growth of such tails observed in this study, with the images taken from a high-speed video. While the local patch cavitation persists after the bubble has passed, the flow ultimately re-attaches to the hydrofoil surface.

The bubble may also cause a local pressure disturbance, as suggested by Briançon-Marjollet *et al.* (1990). The flow near the midchord is in tension and as the bubble passes, an adverse pressure gradient will exist upstream of the bubble. It is suggested that this pressure gradient may cause a local detachment of the boundary layer which could produce a local turbulent region. Our observations suggest that this pressure perturbation does not by itself produce the local turbulent spot. Bubbles which traveled wholly above the surface did not produce the turbulent spot, yet these bubbles were separated by only a thin liquid layer approximately two to three boundary layers thick. Such a bubble would still be expected to influence the boundary layer through local changes in the potential pressure field, but no evidence was seen that these bubbles would generate a turbulent region. Only the bubbles forming a wedge close to the foil surface produced a disturbance in the boundary layer.

Surface nuclei could be stimulated to cavitation by the pressure fluctuations of the turbulent spot. Huang & Peterson (1976) report that pressure fluctuations in a turbulent boundary layer can be on the order of 20% of the dynamic pressure, $1/2\rho U_o^2$, and these pressure fluctuations are strong enough to induce local cavitation in the cores of turbulent vortices. Figure 8(*c*) shows such an event where a small bubble induced from the surface nucleus forms in the turbulent region created by a passing bubble. This small bubble grows out of the boundary layer and forms a small local attached cavity near the site of the surface nucleus. Ultimately, the bubble will detach from the surface and move downstream, and the surface cavity will disappear.

Some cavitation bubbles were observed to induce a broad region of attached cavitation that was left upstream as they passed close to the hydrofoil, although these events occurred infrequently for the case of the naturally occurring boundary layer. We believe that in these cases, the bubble instigated a local turbulent region only in its path as it passed over the boundary layer, and this turbulent region would then cause a local patch of attached cavitation. This phenomena is discussed next.

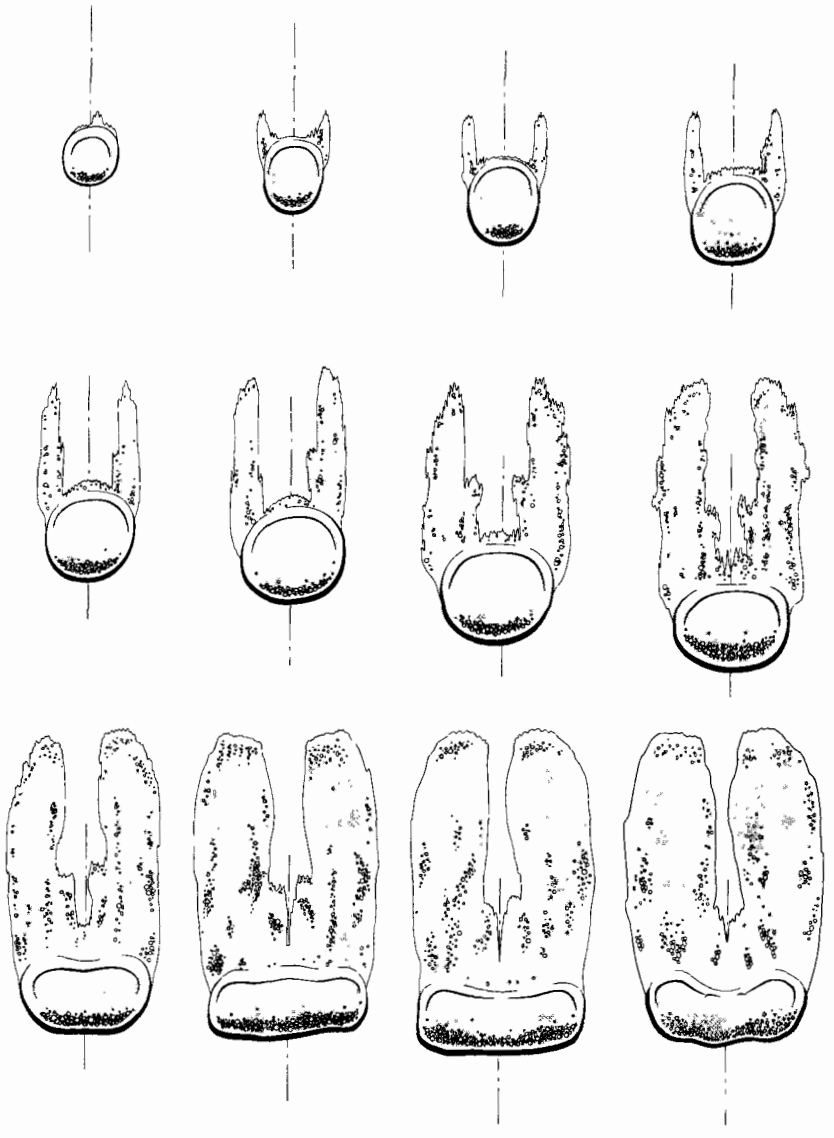

FIGURE 12. The spanwise flow and turbulent transition may lead to a local three-dimensional boundary layer separation at the spanwise edges of the bubble. This separated zone can fill with vapour supplied by the original bubble forming local partial cavitation. A schematic diagram of this process derived from a high-speed video is shown here.

4.3. *Interactions of travelling bubbles with a stimulated boundary layer*

The boundary layer was stimulated to turbulence through the application of roughness at the leading edge, and nuclei were generated near the leading edge of the hydrofoil, as described above. Figure 13(*a*) shows a series of bubbles which demonstrate the growth of travelling cavitation as it occurs over the turbulent boundary layer, and figure 13(*b*) shows a schematic of the process. Vapour is sheared off the bottom of the bubbles, and a region of cavitation remains upstream. Note that the local patch cavitation does not exhibit the 'tail' structure described above. Instead, the region of vapour is almost uniform across the bubble span.

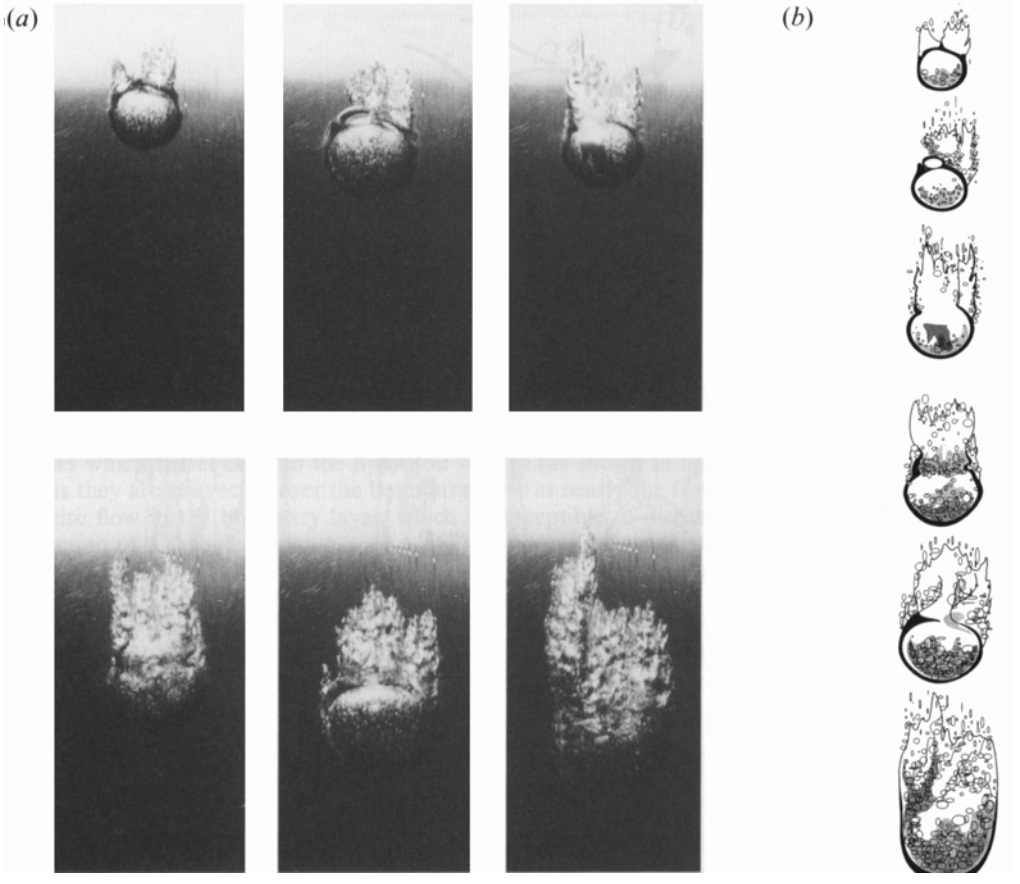

FIGURE 13. (*a*) Plan view of several bubbles as they pass over the turbulent boundary layer on the hydrofoil. Vapour from the bottom surface of the bubble is sheared off and entrained in the turbulent boundary layer, and a region of patch cavitation is produced upstream of the bubble. (*b*) A schematic diagram of the growth process in (*a*).

As the bubble passes over the turbulent region, the bottom of the bubble may act as a 'macroscopic nucleus' providing a source of vapour which can be entrained by the turbulent vortices, and the growth of vapour bubbles within the vortices led to a local three-dimensional boundary layer separation. After the bubble passes, the local detachment region often grows in the spanwise direction, but these regions do not persist indefinitely and are ultimately swept away by a reattachment of the liquid flow to the hydrofoil surface. Often it was not possible to observe the clear surface of a hemispherical bubble, and only the patch of cavitation was observed to grow and collapse, as shown in figure 14. In these cases, the initial nucleus may have led to inception within the boundary layer directly. The growth and collapse time of the cavity patches is approximately 12 ms, which is about twice the total growth and collapse time of a travelling bubble.

Travelling cavitation events of this type were observed by Kuhn de Chizelle *et al.* (1995) on axisymmetric headforms. As the size of the headforms increased, the likelihood that travelling cavitation events would produce local patches increased, and at the highest Reynolds number, patch cavities were primarily observed. It is likely that as the Reynolds number of the flow increased, the boundary layer underwent

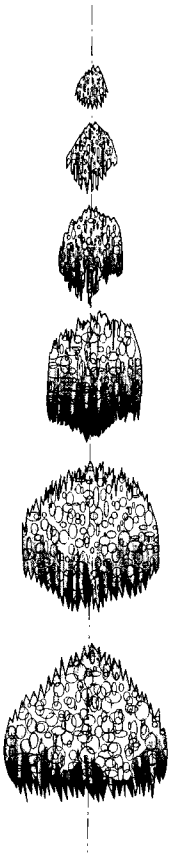

FIGURE 14. A schematic diagram showing the shape evolution of patch cavitation as it passes over the turbulent boundary layer on the hydrofoil. The figure was derived from a high-speed video.

natural transition on the larger headforms much closer to the region of tension. Thus, travelling cavitation events were more likely to interact with a turbulent boundary layer in the manner described above.

4.4. *Acoustic emission of travelling bubbles*

Ceccio & Brennen (1991), and Kuhn de Chizelle *et al.* (1995) examined the acoustic emission of naturally occurring cavitation bubbles. Single cavitation bubbles may produce an acoustic pulse upon collapse, and the intensity of the acoustic emission is dependent on the surrounding flow. Travelling bubbles which are associated with local attached cavitation do not, on average, produce as strong an acoustic emission as simply hemispherical bubbles. Similar results were observed in this study. Figure 15 presents a comparison of the acoustic impulse produced by single travelling cavitation bubbles as they passed over the naturally occurring and fully stimulated boundary layers. The acoustic impulse is defined as

$$I = \int_{t_1}^{t_2} P_A \mathrm{d}t,$$

where P_A is the pressure pulse generated by a collapsing bubble. The times t_1 and t_2 were chosen to exclude the shallow pressure rise before collapse and the

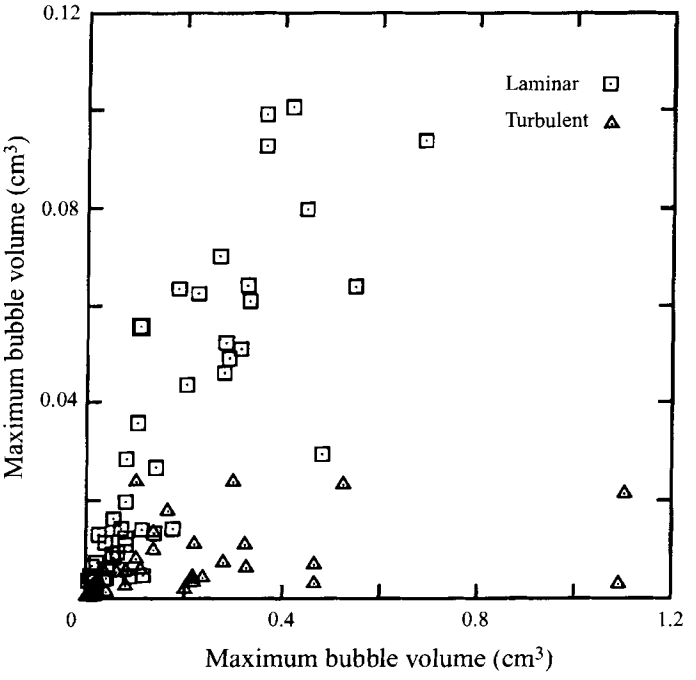

FIGURE 15. A plot of acoustic impulse versus bubble volume for bubbles travelling over the naturally occurring boundary layer and over the turbulent boundary layer.

reverberation produced after collapse (Ceccio & Brennen 1991). The maximum volume for each bubble was determined by measuring the bubble base diameter from photographs of the individual bubbles and from that calculating the volume of an equivalent spherical cap. Bubbles moving over the naturally occurring boundary layer consistently produce a larger acoustic impulse than those which were produced over the turbulent boundary layer. In the latter case, these bubbles almost always were associated with local attached cavitation. These results are consistent with those of Kuhn de Chizelle *et al.* (1995) who also found that bubbles associated with patch cavitation do not produce a strong acoustic emission.

5. Results: interaction of travelling bubbles with the attached cavity

With a reduction in cavitation number, attached cavitation formed at the midchord of the untripped hydrofoil, and individual travelling bubbles were created and observed as they interacted with the attached cavity. As reported by Briançon-Marjollet *et al.* (1990), the bubbles often sweep away a portion of the attached cavity, and in cases where enough naturally occurring nuclei were present in the free-stream, no attached cavitation would form due to the continual sweeping action of the travelling bubbles.

Figure 16(*a*) presents a series of photographs revealing different stages of the sweeping process for several bubbles, and figure 16(*b*) is a schematic representation. Travelling bubbles which swept away the cavity have a relatively constant volume, as evidenced by high-speed photography. The bubbles pass over the cavity interface without initially disturbing it since the original finger cavities are often still visible through the clear interface of the bubble. After the bubble is approximately one to

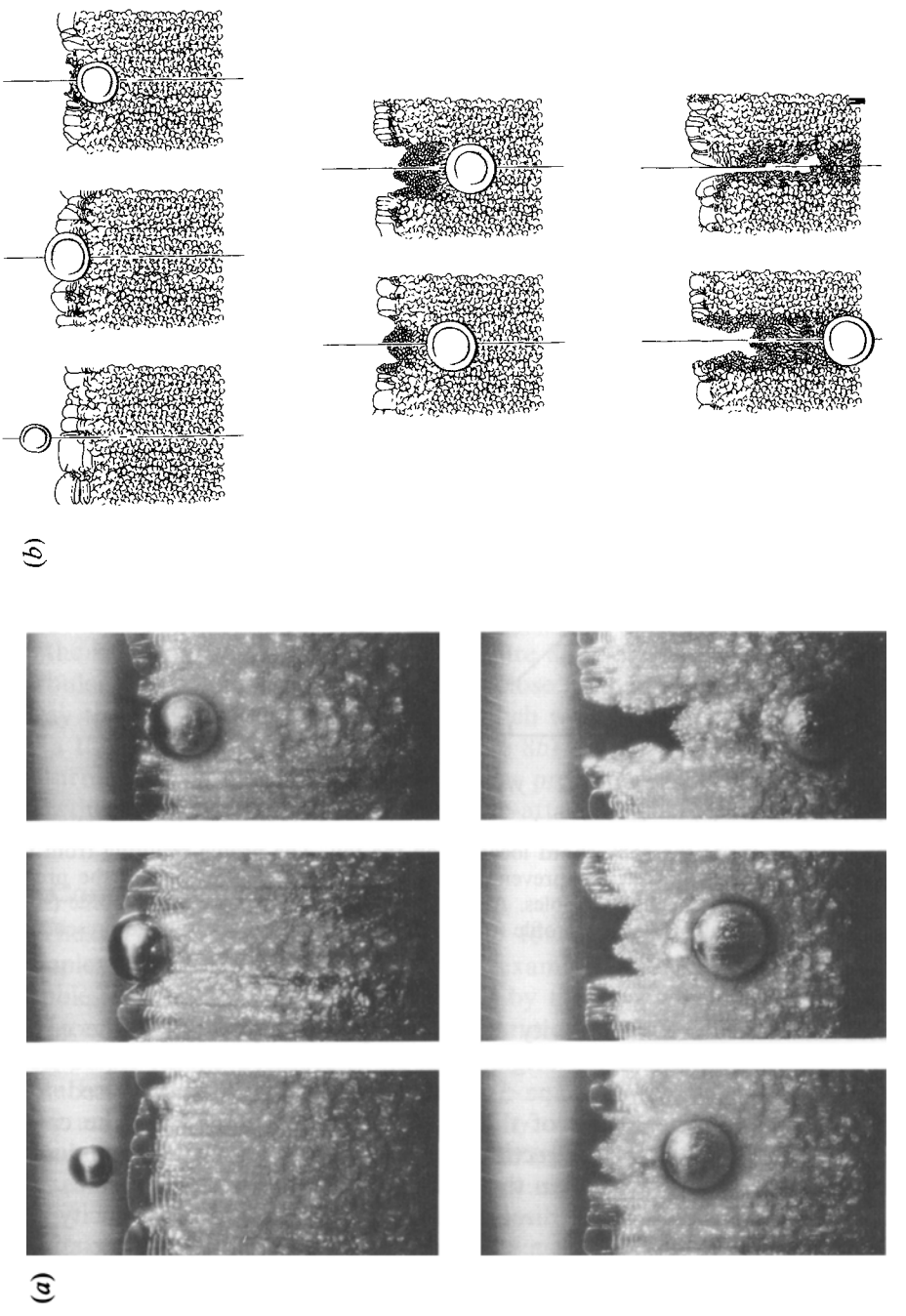

FIGURE 16. (*a*) Images of several bubbles showing the process of cavity sweeping. The bubble first passes over the cavity without disturbing it, and the sweeping action occurs after the bubble has passed downstream. Note the 'fork'-shaped portion of the cavity initially swept away. (*b*) A schematic diagram of the sweeping process.

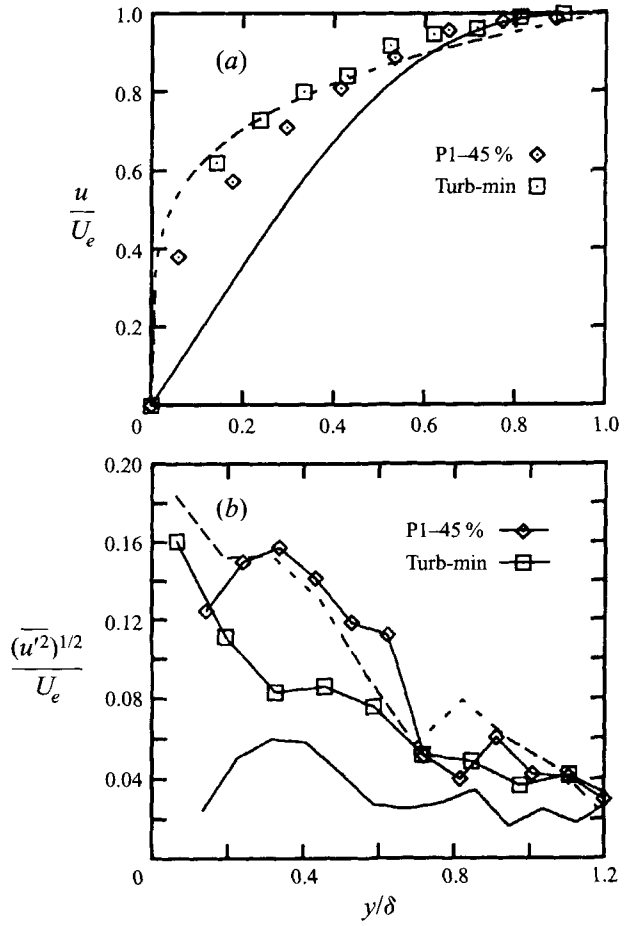

FIGURE 17. A comparison of four boundary layer profiles (*a*) and RMS velocity fluctuations in the streamwise direction (*b*) at the 45% chord location on the foil. The profile resulting from the minimum amount of tripping necessary to prevent laminar separation is compared to the profile resulting from the passage of travelling bubbles. Also plotted is the laminar velocity profile (solid line) and the stimulated turbulent velocity profile (dashed line) which exist without the presence of the travelling bubbles.

two diameters downstream of the cavity separation point, a portion of the cavity extending the spanwise extent of the original bubble is replaced by the liquid flow. This region takes on a 'fork'-like shape as the attached cavity is suppressed to a greater extent at the spanwise edges of the newly reattached zone, and the cavity begins to recede in the streamwise direction. However, this reattached liquid strip soon disappears as the cavity recloses in the spanwise direction from both sides. The cavity is swept away in the streamwise direction at nearly the free-stream velocity, and the sides of the cavity close back with a speed roughly 5 to 10% of the free-stream velocity.

The mechanism for the sweeping action is directly related to the production of the turbulent region upstream of the travelling bubble. It was shown in §3.2 that stimulation of turbulence in the boundary layer prevents the formation of an attached cavity at the midchord. Furthermore, the passage of the travelling bubbles over the laminar boundary layer will produce a local turbulent region as discussed above

in §4.2. Consequently, the sweeping action occurs as the region of bubble-induced turbulence convects over the attached cavity.

The detailed observations of the sweeping process are consistent with this explanation. First, the delay between the passage of the bubble and the sweeping action indicates that the attached cavity was not suppressed directly by the bubble. Second, the 'forked' structure of the initial reattachment zone is consistent with our schematic picture of the growth of the turbulent region behind the bubble presented in figure 9. Lastly, the intensity of the turbulent region upstream of the bubble is sufficient to cause reattachment of the cavity. Figure 17 shows a comparison between the velocity profiles (*a*) and streamwise velocity fluctuations (*b*) for the stimulated boundary layer which is just sufficient to prevent an attached cavity and the boundary layer upstream of the travelling bubble. Also plotted are the fitted curves for the laminar and turbulent velocity profiles for the flow without travelling bubbles. The disturbance of the boundary layer caused by the bubble passage is similar to that of the boundary layer produced by minimal tripping. Indeed, the velocity fluctuations upstream of the bubble are on the same order as the fully tripped boundary layer. Thus, by producing a concentrated region of turbulence, the bubble has created a flow which is sufficient to prevent a separated boundary layer and thus suppress an attached cavity. This type of bubble/boundary layer interaction was suggested by Briançon-Marjollet *et al.* (1990).

Travelling bubbles passing close to the attached cavity might also be expected to produce pressure gradients in the potential outer flow, and Briançon-Marjollet *et al.* (1990) have suggested that the adverse pressure gradient caused by the bubble passage may be responsible for cavity re-attachment. However, only bubbles travelling close to the hydrofoil surface (as shown in figure 8*a*) were observed to induce a region of turbulence, and only bubbles travelling close to the surface were observed to sweep away the cavity. Conversely, bubbles which were wholly separated from the surface by a thin liquid layer (as shown in figure 8*b*) simply passed over the cavity without disturbing it. Thus, we do not believe that pressure gradients induced by the bubble growth or passage are sufficient for the re-attachment of the cavity.

6. Conclusions

The physical mechanisms responsible for cavitation scale effects can be quite complex. In the present study we have examined the processes by which travelling bubbles can influence and be influenced by the viscous flow near a solid cavitating surface. These interactions can be summarized as follows:

(i) Travelling bubbles moving close to a solid surface can stimulate local regions of turbulent flow in an unstable laminar boundary layer by 'squeezing' the boundary layer and thus creating streamwise vorticity.

(ii) These transient turbulent regions can prevent the formation of a laminar separation and can temporarily eliminate a region of attached cavitation.

(iii) Travelling bubbles can stimulate local attached cavitation through the generation of this transient region of turbulence either by stimulation of previously sub-critical surface nuclei or through the creation of local, three-dimensional separated regions.

(iv) Travelling bubbles interact strongly with a turbulent boundary layer producing a local separated region of patch cavitation which may ultimately envelop the original bubble. The acoustic emission of such travelling cavitation events is substantially reduced.

Since travelling bubbles are directly related to the free-stream nuclei population, these mechanisms may result in 'water quality' scale effects. Similarly, the differences between travelling cavitation occurring over laminar and turbulent boundary layers provides a mechanism for a viscous scale effect.

It is important to note, however, that cavitation may result from the separation of bluff objects or as a result of severe adverse pressure gradients. Also, the distance between the location of cavity separation and the location of minimum pressure may be quite small, as is often the case for leading-edge cavitation on thin sections. In these cases, the attached cavitation would not be influenced by the mechanisms described here, and the nuclei population would not be expected to strongly influence the sheet cavity inception.

The authors would like to acknowledge the substantial assistance of Po-Wen Yu and Ann Tassin in the completion of the experiments. This work was supported by the Office of Naval Research under contract N00014-91-J-1063 with Dr Edwin Rood as the contract monitor.

REFERENCES

ADRIAN, R. J. 1991 Particle-image techniques for experimental fluid mechanics. *Ann. Rev. Fluid Mech.* **23**, 261–304.

ARAKERI, V. H. 1975 Viscous effects on the position of cavitation separation from smooth bodies. *J. Fluid Mech.* **68**, 779–799.

ARAKERI, V. H. & ACOSTA, A. J. 1973 Viscous effects in the inception of cavitation on axisymmetric bodies. *Trans. ASME* I: *J. Fluids Engng* **95**, 519–527.

BRENNEN, C. E. 1969 A numerical solution of axisymmetric cavity flows. *J. Fluid Mech.* **37**, 671–688.

BRENNEN, C. E. 1970 Cavity surface wave patterns and general appearance. *J. Fluid Mech.* **44**, 33–49

BRENNEN, C. E. 1995 *Cavitation and Bubble Dynamics*. Oxford University Press.

BRIANÇON-MARJOLLET L., FRANC, J. P. & MICHEL, J. M. 1990 Transient bubbles interacting with an attached cavity and boundary layer. *J. Fluid. Mech.* **218**, 355–376.

CANTWELL, B., COLES, D. & DIMOTAKIS, P. 1978 Structure and entrainment in the plane of symmetry of a turbulent spot. *J. Fluid Mech.* **87**, 641–676.

CECCIO, S. L. & BRENNEN, C. E. 1991 Observations of the dynamics and acoustics of travelling bubble cavitation. *J. Fluid. Mech.* **233**, 633–660.

ELLIS, A. T. 1952 Observation on cavitation bubble collapse. *Rep.* 21-12. California Institute of Technology, Hydrodynamics Lab.

FRANC, J. P. & Michel, J. M. 1985 Attached cavitation and the boundary layer: experimental investigation and numerical treatment. *J. Fluid Mech.* **154**, 63–90.

FRANC, J. P. & MICHEL, J. M. 1988 Unsteady attached cavitation on an oscillating hydrofoil. *J. Fluid Mech.* **193**, 171–189.

GATES, E. M., BILLET, M. L., KATZ, J., OOI, K. K., HOLL, W. & ACOSTA, A. J. 1979 Cavitation inception and nuclei distribution – joint ARL-CIT experiments. *Rep.* E244-1. California Institute of Technology, Division of Engineering and Applied Science.

GINDROZ, B. & BILLET, M. L. 1994 Nuclei and propeller cavitation inception. In *Cavitation and Gas-Liquid Flow in Fluid Machinery and Devices*. ASME FED, vol. 190, pp. 251–260.

HINZE, J. O. 1975 *Turbulence*. McGraw Hill.

HUANG, T. T. & PETERSON, F. B. 1976 Influence of viscous effects on model/full-scale cavitation scaling. *J. Ship Res.* **20**, 215–223.

JAFFE N. A., OKAMURA, T. T. & SMITH, A. M. O. 1970 Determination of spatial amplification factors and their application to predicting transition. *AIAA J.* **8**, 301–308.

KODOMA, Y., TAMIYA, S. & KATO, H. 1978 The effect of nuclei on the inception of bubble and sheet cavitation on axisymmetric bodies. *Proc. Intl ASME Symp. on Cavitation Inception, New York, Dec. 1979*, pp. 75–86.

KUHN DE CHIZELLE, Y., CECCIO, S. L. & BRENNEN, C. E. 1995 Observations and scaling of travelling bubble cavitation. *J. Fluid Mech.* **293**, 99–126.

KUIPER, G. 1981 Cavitation inception on ship propeller models. PhD dissertation, Netherland Ship Model Basin.

LIU, Z. & BRENNEN, C. E. 1994 The relation between the nuclei population and the cavitation event rate for cavitation on a schiebe body. In *Cavitation and Gas-Liquid Flow in Fluid Machinery and Devices.* ASME FED, vol. 190, pp. 261–266.

MEULEN, J. H. J. VAN DER 1980 Boundary layer and cavitation studies of NACA 16-012 and NACA 4412 hydrofoils. *Proc. 13th Symp. on Naval Hydrodyn., Tokyo*, pp. 195-219. National Academy Press.

MEULEN, J. H. J. VAN DER & RENESSE, R. L. VAN 1989 The collapse of bubbles in a flow near a boundary. *Seventeenth Symp. on Naval Hydrodynamics, The Hague*, pp. 379–392. National Academy Press

MEYER, R. S., BILLET, M. L. & HOLL, J. W. 1992 Freestream Nuclei and travelling Bubble Cavitation. *Trans ASME* I: *J. Fluids Engng* **114**, 672–679.

ROOD, E. P. 1991 Mechanics of cavitation inception-Review. *Trans ASME* I: *J. Fluids Engng* **113**, 163–175.

SAVAGE, M. D. 1977*a* Cavitation in lubrication. Part 1. On boundary conditions and cavity–fluid interfaces. *J. Fluid Mech.* **80**, 743–755.

SAVAGE, M. D. 1977*b* Cavitation in lubrication. Part 2. Analysis of wavy interfaces. *J. Fluid Mech.* **80**, 757–767.

TASSIN, A. L., LI, C. Y., CECCIO, S. L. & BERNAL, L. P. 1995 Velocity field measurements of cavitating flows. *Exps. Fluids* **20**, 125–130.

WEITENDORF, E. & TANGER, H. 1993 Cavitation investigations in two conventional tunnels and the hydrodynamics and cavitation tunnel HYKAT. *Proc. Intl ASME Symp. On Cavitation Inception, New Orleans, Dec. 1993*, pp. 73–89.

WHITE, F. M. 1974 *Viscous Fluid Flow.* McGraw Hill.

WYGNANSKI, I., SOKOLOV, M., & FRIEDMAN, D. 1976 On a turbulent 'spot' in a laminar boundary layer. *J. Fluid Mech.* **78**, 785–819.